



Research article

Synthesis and characterization of folate-functionalized silica-based materials and application for bioimaging of cancer cells

Yalda Zare^{a,1}, Maral Maghsoudi-Salek^{b,1}, Zahra Golsanamlu^c,
Abolghasem Jouyban^d, Jafar Soleymani^{d,*}, Hassan Bagherpour-Shamloo^d^a Drug Applied Research Center, Tabriz University of Medical Sciences, Tabriz, Iran^b Liver and Gastrointestinal Research Center, Tabriz University of Medical Sciences, Tabriz, Iran^c Department of Pharmaceutical Chemistry, Faculty of Pharmacy, Tabriz University of Medical Sciences, Tabriz, Iran^d Pharmaceutical Analysis Research Center, Tabriz University of Medical Sciences, Tabriz, Iran

ARTICLE INFO

Keywords:Bioimaging
Targeted-imaging
Cell membrane glycoprotein
Membrane receptor
Circulating tumor cells (CTCs)

ABSTRACT

Early-stage detection is a vital factor in the later treatment and prognosis of cancer. Enhancing the sensitivity and specificity of the cancer detection pathological and experimental approaches can affect the morbidity and mortality of this disease. A folic acid (FA)-functionalized silica quantum dots (SiQDs)/KCC-NH₂@SiO₂ nanomaterials were synthesized and characterized as a bioimaging agent of the MCF 7 cancer cells. These nanoparticles showed biocompatible nature with specificity towards folate receptor (FR)-overexpressed MCF 7 cancer cells. Viability findings suggested that the SiQDs/KCC-NH₂@SiO₂/FA nanomaterials have nontoxic nature towards the cells in the concentration of 200 µg/mL. Fluorescence microscopy images were utilized to estimate the cell internalization of the nanoparticles and further verified by the flow cytometry technique. The differentiation ability of the nanoparticles was also approved by incubation with FR-negative HEK 293 normal cells. The SiQDs/KCC-NH₂@SiO₂/FA nanoparticle exhibited high stability, bright and high quantum yield fluorescence emission, proposing as a high-quality material for *in vivo* bioimaging of FR-overexpressed circulating tumoral cancer cells (CTCs).

1. Introduction

Cancer is one of the most severe worldwide health problems which is dangerous for human beings. According to the American Cancer Society reports, there exist 19.3 million new cases of cancer and approximately 10 million deaths in 2020. The prevalence of this disease is increasing fast, we may face 28.4 million cases in 2040 which is 47% more than in 2020 [1,2]. Tumor metastasis is one of the critical processes in cancer disease. During tumor metastasis step, a new tumor forms very similarly morphology to the primary tumor cells. About 90% of deaths happen because of the migration of tumor cells which separate from tumor tissue and release into the bloodstream and lymph nodes. These cells are called circulating tumor cells (CTCs) which are considered an important biomarker for the diagnosis and management of cancer [3]. However, only a low concentration of tumor cells is presented in the blood, therefore high

* Corresponding author.;

E-mail addresses: jsoleymanii@gmail.com, soleymanij@tbzmed.ac.ir (J. Soleymani).¹ These authors equally contributed.

sensitive detection of tumor cells is very challenging [4]. Numerous methods and techniques have been used for cancer diagnosis using biomarkers and bioimaging. However, imaging of solid tumors is still the main technique in clinical and preclinical applications [5–8].

Macroscopic and molecular imaging techniques such as magnetic resonance imaging (MRI), computed tomography (CT), single-photon emission computed tomography (SPECT), ultrasound (US), etc. are currently applied in the bioimaging of solid tumors that provide various beneficial features. However, some of these techniques possess some pitfalls such as high cost, inconvenient procedures, false positive/negative and qualitative results, etc. which prevent their applications for fast imaging purposes. Nanotechnology-based imaging methods are new-fashioned methods that have attracted interest in medical affairs and were studied on large scales in research institutions. Fluorescence bioimaging approaches offer high sensitivity and simple imaging approaches without the need for very skilled persons [9]. New bioimaging methods are applied novel advanced materials modified with molecules to enhance the specificity of the bioimaging method. A way to provide specific bioimaging is employing of receptors that are over-expressed on the surface of the cancer cells rather than normal cells [10–12].

Recent studies showed that targeted detection and imaging of cancer cells are very useful for the on-time discrimination of cancerous tissues [13]. Targeted detection means that the detection platform can only attach to the target analyte with high selectivity. Folic acid (FA) as a water-soluble vitamin is very important agent for health and its reduced levels may lead some serious health problems [14,15]. FA can be employed as one of important ligands for labeling cancer cells due to their selective binding to the folate receptor (FR). Compared to other ligands, FA has noticeable stability and low molecular weight, and also it can be easily attached to other particles. FR is a glycoprotein with a high affinity to FA and has three different forms: α , β , and γ . The α and β forms of FR can be attached to the cell membrane by glycosylphosphatidylinositol anchors (GPI), on the other hand, the γ form can be found in hematopoietic cells [16–18]. Different nanomaterials such as gold nanoparticles, silver nanoparticles, silica nanoparticles, quantum dots, etc. have been conjugated to FA molecules to be used as smart cell-specific materials [19–24]. Among the numerous nanoparticles, silica nanoparticles have been widely used because of their special properties such as large surface area, noticeable thermal conductivity, and biocompatibility. These unique features make silica nanoparticles effective platforms for different agents of anticancer. To increase the targeting ability, the surface of nanoparticles is mostly modified with different ligands like nucleic acids, peptides, and small molecules. This modification usually leads to form a strong bond between the modified nanoparticles and cancer cells [25,26]. Amine-functionalized fibrous silica (KCC-NH₂) is a favorable nanomaterial for modification and functionalization due to the presence of various active sites [27].

In the current study, the FA-functionalized silica quantum dots (SiQDs)/KCC-NH₂@SiO₂/FA nanomaterials were employed as cell targeting materials for bioimaging MCF 7 tumoral cells. The cell uptake of the nanomaterials was evaluated through different techniques where the fluorescence microscopy and flow cytometry techniques were applied for qualitative and quantitative internalization of the nanoparticles, respectively. HEK 293, as a folate receptor negative cell, was regarded as the control group to assay the specificity of the SiQDs/KCC-1-NH₂@SiO₂/FA nanoparticles. The reported bioimaging method was effectively utilized for the recognition of FA-positive MCF 7 cells and also would be applied as a promising platform for reliable differentiation of other FA-overexpressed cancer cells from low-expressed normal ones.

2. Experimental section

2.1. Materials

FA was purchased from Mehr Darou pharmaceutical company (Iran). (3-Aminopropyl)triethoxysilane (APTES, 99%), polyvinyl chloride (PVP), 1-ethyl-3-(3-dimethylaminopropyl) carbodiimide (EDC, 98.0%), N-hydroxysuccinimide (NHS, 98.0%), rhodamine B, tetraethyl orthosilicate (TEOS, 98%), and 3-(4,5-dimethylthiazol-2-yl)-2,5-diphenyltetrazolium bromide (MTT) were provided from Sigma-Aldrich Co. (USA). Cyclohexane, sodium hydroxide (NaOH), hydrochloric acid (HCl), cetyltrimethylammonium bromide (CTAB), sodium ascorbate (SA), toluene, hexanol, ammonia solution, and dimethylsulfoxide (DMSO) were obtained from Merck (Germany). Also, phosphate buffer solution (PBS, 98.0%) and trisaminomethane hydrochloride (Tris-HCl) were purchased from Sigma-Aldrich Company (Germany). Roswell Park Memorial Institute (RPMI) 1640, fetal bovine serum (FBS), and trypsin-EDTA (25%) were obtained from Gibco Co. (UK). All cell lines were provided from the National Cell Bank of Iran (NCBI) in Tehran (Iran).

2.2. Apparatus

Physicochemical features of FA-functionalized SiQDs/KCC-1-NH₂@SiO₂ nanocomposite were checked using different instrumental sets. Fourier transform infrared (FTIR, Bruker model instrument (Billerica, Massachusetts, US)) was used to identify functional groups. Fluorescence spectra were recorded using a JASCO FP 750 spectrofluorometer (Tokyo, Japan). The cellular uptake of FA-functionalized SiQDs/KCC-1-NH₂@SiO₂ nanocomposite was recorded by a fluorescent microscopy (Olympus BX64, Olympus, Japan) with U-MWU2 fluorescence filter (excitation filter BP 330e385, dichromatic mirror DM 400, emission filter LP 420). However, the size and surface state of the FA-functionalized SiQDs/KCC-1-NH₂@SiO₂ were characterized by transmission electron microscopy (TEM), Carl Zeiss LEO 906 electron microscope operated at 100 kV (Oberkochen, Germany), and field emission scanning electron microscopy (FESEM, FEG-SEM MIRA3 TESCAN (Brno, Czech Republic), respectively. Energy dispersive X-ray (EDX) of the FA-functionalized SiQDs/KCC-1-NH₂@SiO₂ were analyzed by a FEG-SEM MIRA3 TESCAN (Brno, Czech Republic). Hydrated size and surface charge of the produced materials were measured using a Malvern particle size analyzer (Malvern, UK). Flow cytometry analyses were done by Cell Quest Pro software (BD Biosciences, San Jose, CA, USA). MTT assay test plate was read using a microplate reader Awareness Technology (Florida, USA).

2.3. Synthesis

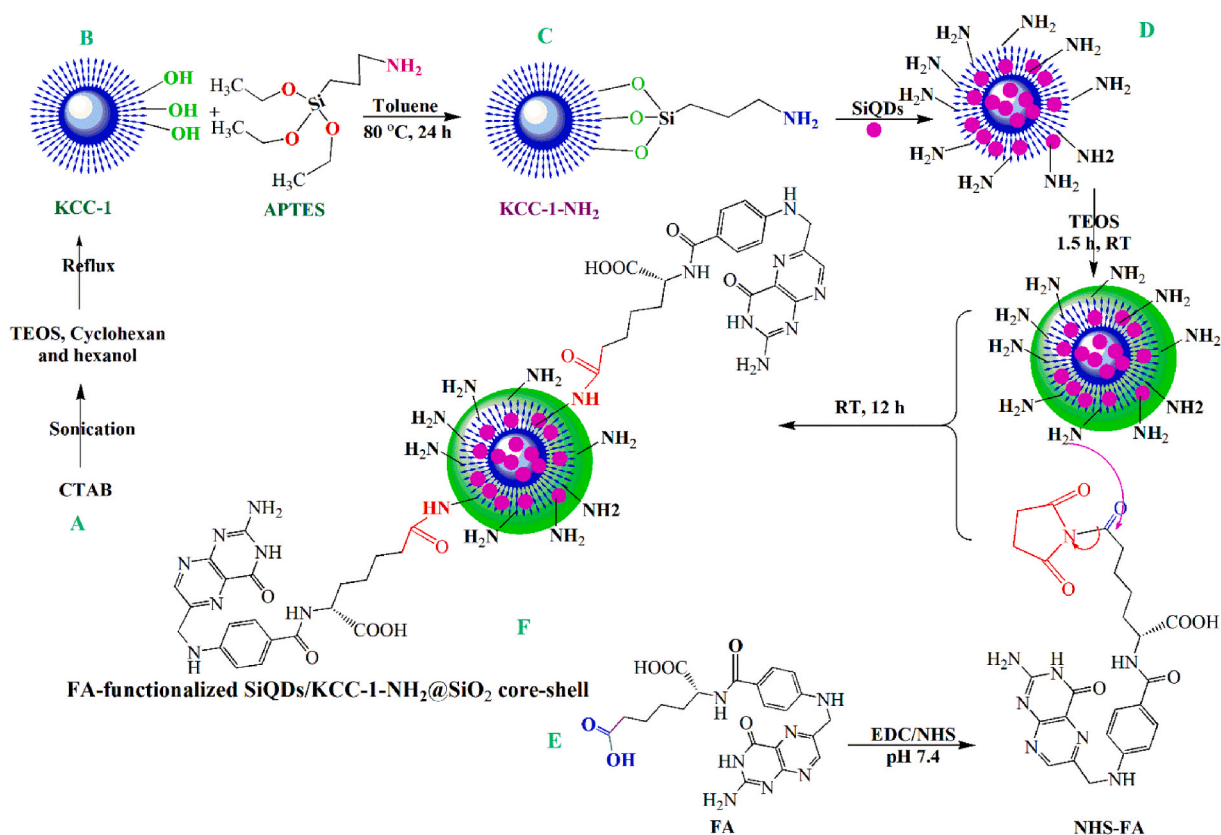
2.3.1. Synthesis of amine functionalized silicon dots (SiQDs)

SiQDs were synthesized by a hydrothermal method previously reported by our group [28]. Firstly, SA (250 mg) was dissolved in about 50 mL of deionized water and then nitrogen aerated for around 30 min to remove dissolved oxygen and named solution I. Then, about 5 mL of solution I was mixed with 4 mL of APTES, and then the solution was agitated at room temperature for at least 0.5 h (solution II). Next, solution II was transferred into an autoclave and then remained at 175 °C for 20 h. To enhance the stability of the produced QDs, PVP (300 mg) was added to the final mixture. After centrifuging, the final mixture was transferred to dialysis bags (1 kDa) to remove byproducts and unconsumed materials.

2.3.2. Preparation of KCC-1 and its amine-functionalized form

KCC-1 dendritic porous composite was produced using a method reported by Bayal et al. [29]. Firstly, CTAB (2 g) was dissolved in 20 mL of deionized water, and then urea (1.2 g) was added to the mixtures and agitated for at least 3 h at 25 °C (flask 1). TEOS (4 g), cyclohexane (60 mL) and hexanol (3 mL) solvents were mixed and gradually added to flask 1 and sonicated for at least 45 min. The production of KCC-1 nanocomposite is started by refluxing the mixture at 120 °C and 80 °C for 4 h and 24 h, respectively. After cooling the mixture to room temperature and centrifuging (10000 rpm, 10 min), the KCC-1 white sediment was collected and washed with water and ethanol several times. Finally, the KCC-1 composite was dried at 60 °C (24 h) and calcined (at 600 °C, 5 h) to eliminate the CTAB template. As a mechanism of the KCC-1 synthesis, urea was used to hydrolyze the TEOS to produce negatively charged $(\text{SiO}_4)^{4-}$ silicate. CTAB molecules induce the silicate to form a self-assembled linear structure where the CTAB molecules help to gather the silicates alongside each other [30].

KCC-1-NH₂ nanocomposite was produced using APTES molecule. Briefly, KCC-1 (40 mg) was added to the dried toluene (2.5 mL) and sonicated to obtain a well-dispersed mixture. Then, APTES (100 μL) was added to the mixture and refluxed at 80 °C for at least 24 h. Finally, the mixture was centrifuged (10000 rpm) and washed with toluene three times and dried to remove toluene molecules (80 °C, 24 h) [31].



Scheme 1. Synthesis steps of SiQDs/KCC-1-NH₂@SiO₂/FA nanoparticle (Step A: synthesis of KCC-1, Step B: synthesis of KCC-1-NH₂, Step C: synthesis of KCC-1-NH₂-SiQDs, Step D: synthesis of KCC-1-NH₂-SiQDs@SiO₂, Step E: activation of FA molecules, and Step F: synthesis of SiQDs/KCC-1-NH₂@SiO₂/FA).

2.3.3. Production of SiQDs/KCC-1-NH₂@SiO₂ composite

Water-dispersible SiQDs (2 mL) were mixed with KCC-NH₂ (5 mL, 5 mg/mL) and stirred for about 3 h at room temperature. The pH of the mixture solution was adjusted to pH 7.8 using NaOH and HCl solutions. In this pH, SiQDs can be homogeneously anchored on the surface of dendrimers of KCC-1-NH₂. After adding about 4 mL water and 2 mL of ammonia solution to the SiQDs/KCC-NH₂ solution and stirring for about 5 min, approximately 0.5 mL of TEOS was further added, and then the mixture was agitated for 1.5 h. The addition of TEOS provides a thin silica shell on the out layer of SiQDs/KCC-NH₂, yielding SiQDs/KCC-NH₂@SiO₂. This shell acts as an effective antifouling layer and enhances the stability of the nanocomposite. The produced SiQDs/KCC-NH₂@SiO₂ nanocomposite were isolated by centrifugation (10000 rpm) and washed with distilled water several times. The produced nanocomposite is stable for at least one month in a refrigerator.

2.3.4. Synthesis FA-NHS

To attach the FA molecules to amine groups of the SiQDs/KCC-NH₂@SiO₂ nanocomposite, it is necessary that the carboxyl groups of FA molecules be activated using EDC/NHS reaction. 3 mg of FA molecules, 3 mg of EDC and 5 mg of NHS were mixed in phosphate buffer pH 7.0 and stirred at room temperature for about 12 h. Finally, the produced FA-NHS molecules were stored at -4 °C.

2.3.5. Preparation of FA-functionalized SiQDs/KCC-1-NH₂@SiO₂ composite

5 mL of SiQDs/KCC-1-NH₂@SiO₂ was added to about 2 mL of FA-NHS and stirred at room temperature for about 12 h. Finally, FA-functionalized SiQDs/KCC-1-NH₂@SiO₂ nanoparticles were dialyzed (3 kDa) against deionized water. The as-prepared materials are stable at 2–8 °C for at least 30 days. All synthesis steps are summarized in [Scheme 1](#).

2.4. Biological tests

2.4.1. Cell culture

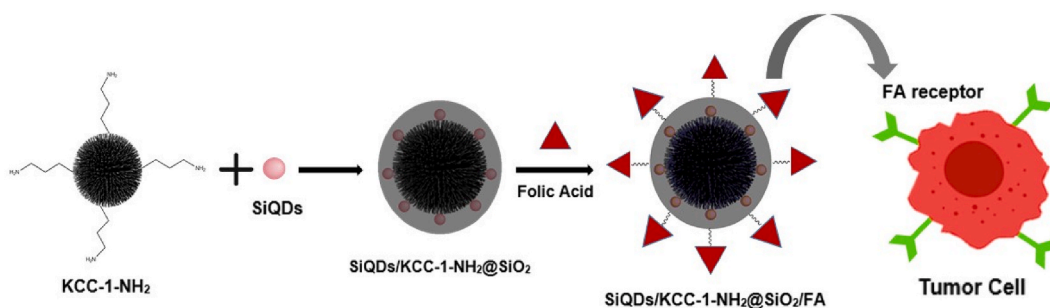
MCF 7 and HEK 293 cell lines were thawed and seeded in the RPMI 1640 medium (10% of FBS and 1% penicillin/streptomycin) supplemented flasks and incubated for days to grow the cells. After appropriate days, the RPMI media was removed, and the cells were washed with PBS (pH 7.4). Next, trypsin solution was added to the flask to separate the cells after incubation for about 5 min. Then, the cells were transported to a 15-mL conical tube and centrifuged to sediment the cells. Finally, fresh RPMI media was added to the cells and dispersed.

2.4.2. Cell viability

The toxicity effect of FA-functionalized SiQDs/KCC-1-NH₂@SiO₂ composite towards MCF 7 cell lines was checked by MTT assay. To do this assay, around 10⁴ MCF 7 cells were seeded into the wells of a 96-well plate and then incubated for at least for 24 h. After that, different concentrations of FA-functionalized SiQDs/KCC-1-NH₂@SiO₂ composite (50–200 µg/mL) were added to the wells and incubated for 6–24 h. Then, about 20 µL of MTT reagent (3 mg/mL) was added and incubated for about 4 h. Next, the wells' liquids were replaced by 200 µL DMSO and incubated for another 30 min. Finally, the absorbance intensity of each well was measured at 570 nm, and cell viability was calculated as the ratio of the absorbances of samples to the control ones.

2.4.3. Cell uptake study

To check the cell uptake of FA-functionalized SiQDs/KCC-1-NH₂@SiO₂ composite, the cell lines were incubated with the nanocomposite at various concentrations and times of incubation. About 5 × 10⁵ of the cells were seeded to the wells of a 6-texture plate. After the attachment of the cells to the bottom of the plate, the wells were treated with FA-functionalized SiQDs/KCC-1-NH₂@SiO₂ nanocomposite. Next, the slides were washed with PBS buffer (pH 7.4). The quantitative and qualitative assessments of FA-functionalized SiQDs/KCC-1-NH₂@SiO₂ nanoparticle uptake were implemented using flow cytometry and fluorescence microscopy, respectively, using a standard approach.



Scheme 2. Schematic FA/FR integration between SiQDs/KCC-1-NH₂@SiO₂/FA and FR-positive cancer cells.

3. Results and discussion

3.1. Structural and morphological properties of SiQDs/KCC-1-NH₂@SiO₂/FA nanocomposite

Fig. 1(a) and (b) show the SEM images of SiQDs/KCC-1-NH₂@SiO₂/FA nanocomposite. As expected, the general shape of nanocomposite is affected by the KCC-1-NH₂ nanoparticles with dendrimer-like structures. Fig. 1(c) and (d) are the demonstration of FESEM images of SiQDs/KCC-1-NH₂@SiO₂/FA. The produced SiQDs/KCC-1-NH₂@SiO₂/FA particles are in a spherical structure in which a thin layer of SiO₂ covers SiQDs/KCC-1-NH₂ with a total size of around 250 nm. SEM size is close to the DLS size of SiQDs/KCC-1-NH₂@SiO₂/FA which presents the hydrated diameter of composite (290 nm) (F. 1S). EDX data of the SiQDs/KCC-1-NH₂@SiO₂/FA approved the existence of C, N, O, and Si with 44.5, 9.55, 39.7, and 6.2 percentages, respectively (F. 2S and T. 1S). The zeta potential value of the SiQDs/KCC-1-NH₂@SiO₂/FA composite is +34.8 mV which is mainly caused by FA molecules presented on the shell surface of SiQDs/KCC-1-NH₂@SiO₂/FA. In general, amine-functionalized materials are in cationic forms in neutral and acidic pHs. In neutral pH, upon adding of SiQDs (with amine functional groups with -12.6 mV) to KCC-1-NH₂, the zeta potential of SiQDs/KCC-1-NH₂ is turned into more negative charges; however, after adding of SiO₂ layer and FA molecules, a final zeta potential value of +34.8 mV is obtained (T. 2S) [32,33]. The vibrational stretching of Si-O-R is responsible for the appearance of absorption bands between 1000 and 1200 cm⁻¹. However, the spectra in the 600-800 cm⁻¹ and 1579-3356 cm⁻¹ ranges are related to the stretching and vibrational modifications of N-H bonds. The absorption spectrum at around 1050 cm⁻¹ denotes to the Si-O-Si asymmetric stretching vibrations [34]. Si-OH peak is observed at 960 cm⁻¹ which represents the stretching vibration and asymmetric bending. Furthermore, the peak at around 1510 cm⁻¹ is assigned to the amide II bonds between the carboxyl moiety of FA and the amine group of the KCC-1-NH₂. F. 3S presents the FTIR spectra of FA, KCC-1-NH₂, and SiQDs/KCC-1-NH₂@SiO₂/FA.

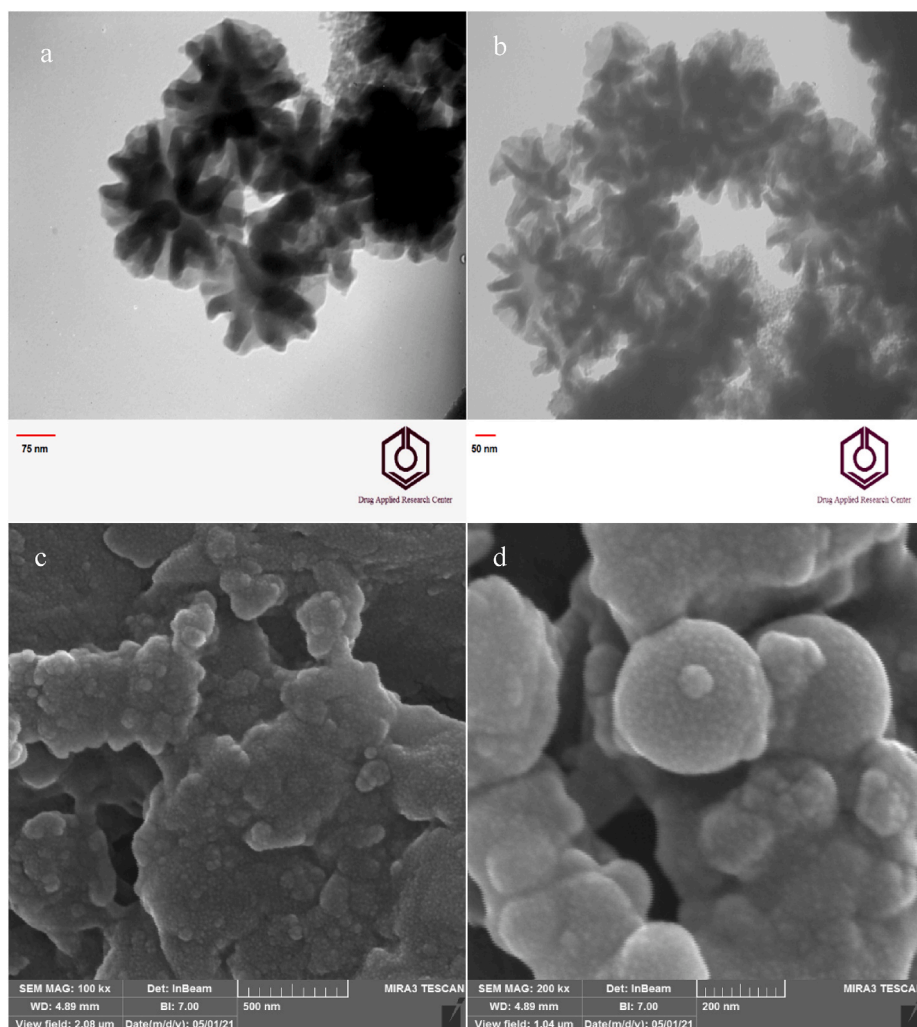


Fig. 1. TEM (a and b) and FESEM (c and d) images of SiQDs/KCC-1-NH₂@SiO₂/FA.

3.2. Spectroscopic properties SiQDs/KCC-1-NH₂@SiO₂/FA

Fig. 2a reports UV spectra of SiQDs and SiQDs/KCC-1-NH₂@SiO₂/FA nanocomposite. An absorption at around 280 nm was observed in SiQDs which could be ascribed to $n-\pi^*$ electron transitions. However, SiQDs/KCC-1-NH₂@SiO₂/FA spectrum showed two absorptions at 350 nm and 500 nm which 350 nm is provided by $\pi-\pi^*$ electron transitions and responsible for the fluorescence emission of SiQDs/KCC-1-NH₂@SiO₂/FA nanocomposite [34]. The SiQDs/KCC-1-NH₂@SiO₂/FA exhibited blue absorption under UV lamp irradiation. Excitation and emission spectra of the SiQDs/KCC-1-NH₂@SiO₂/FA are accessible in F-4S.

The fluorescence emission peak of SiQDs was changed from 436 nm to 466 nm after their attachments to the KCC-1-NH₂@SiO₂/FA 3D-structure (F. 5S). Upon changing of the excitation wavelength from 300 to 400 nm, the luminescence of SiQDs/KCC-1-NH₂@SiO₂/FA changed in which the emission intensity was increased up to 360 nm and then decreased to a minimum amount at 400 nm. In addition, the emission wavelengths of SiQDs/KCC-1-NH₂@SiO₂/FA nanoparticles have been altered to the longer wavelengths, which contradicts Kasha's rule (F. 6S). If the singlet states of the excited level (S1 and S2) have substantial energy gaps, the emission wavelengths do not follow the general rule [35]. The emission wavelength may also be affected by many excited states and the sluggish relaxation rate of the medium [36].

3.3. Influence of pH on the fluorescence and absorbance of the SiQDs/KCC-1-NH₂@SiO₂/FA

The pH of media has an important effect on fluorescent and absorption wavelengths and intensity of SiQDs/KCC-1-NH₂@SiO₂/FA. Fig. 2b shows how pH can affect the absorbance intensity and wavelength of the nanocomposite. The absorbance is increased by increasing pH value up to around pH 7 and then a mild decreasing trend is obtained up to near pH 10.5. However, there is no blue or red shift in the absorption maxima of the nanocomposite.

Moreover, fluorescence emission intensity and wavelength of the SiQDs/KCC-1-NH₂@SiO₂/FA can be affected by the pH of the media. Fig. 3 and F. 7S depict that the fluorescence emission peaks wavelength was changed from 445 nm (pH 3.5) to 460 nm (pH 10.5). Also, the emission intensity was increased from pH 2.5 to 8.5.

3.4. Quantum yield (QY) estimation

QY of SiQDs/KCC-1-NH₂@SiO₂/FA was calculated using tyrosine (Tyr) as the reference substance [37] with a QY of about 14% in water. To determine relative QY, the concentration of SiQDs/KCC-1-NH₂@SiO₂/FA and Tyr were regulated to provide absorbance below 0.1. Then, their fluorescence emissions were measured at the obtained concentrations. Finally, the QY of the

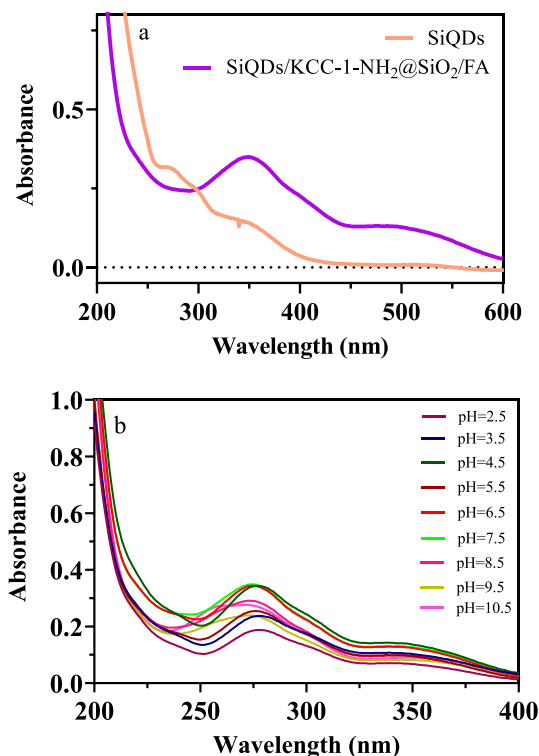


Fig. 2. UV spectra of SiQDs, SiQDs/KCC-1-NH₂@SiO₂/FA AuNPs (a) and pH influence on the absorbance peak and intensity of the SiQDs/KCC-1-NH₂@SiO₂/FA AuNPs (b).

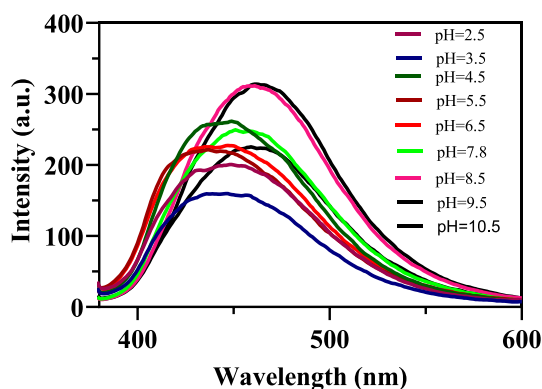


Fig. 3. Influence of pH on the fluorescence emission of SiQDs/KCC-1-NH₂@SiO₂/FA (Excitation wavelength: 360 nm).

SiQDs/KCC-1-NH₂@SiO₂/FA was calculated using the below equation.

$$QY_S = QY_R \left(\frac{A_R}{A_S} \right) \left(\frac{F_S}{F_R} \right) \left(\frac{\eta_S}{\eta_R} \right)^2$$

here “S” and “R” are SiQDs/KCC-1-NH₂@SiO₂/FA and Tyr, and QY_S and QY_F are quantum yields of nanocomposite and Tyr, respectively. A, F and η describe to the absorbance, fluorescence peak area and refractive index of solvent (=1 for water), respectively. The QY of SiQDs/KCC-1-NH₂@SiO₂/FA has been calculated at about 28%, near the reported values (21%) [38]. A comparison between the QYs is presented in T. 3S. A little increase in QY was observed after the addition of the KCC-1 which is mainly caused by the intrinsic 3D structure of the KCC-1 material, collecting more QDs on a spot on its surface.

3.5. Targeting of cancer cells

3.5.1. Toxicity assay

The cytotoxicity of SiQDs/KCC-1-NH₂@SiO₂/FA was checked against MCF 7 cancer lines using the MTT assay. The cytotoxicity of SiQDs/KCC-1-NH₂@SiO₂/FA was determined at 50, 100, 150, and 200 μ g/mL concentrations for 6, 12, 18, and 24 h (F. 8S). Results revealed that the cell survival rate was eventually high at the first 12 h of incubation with mean viability of about 90% for all concentrations of SiQDs/KCC-1-NH₂@SiO₂/FA. However, the viability values decreased by around 75% after 18 h and 24 h incubation times. The results proved that the MCF 7 cell survival rate was not affected by SiQDs/KCC-1-NH₂@SiO₂/FA at the tested concentration, and these materials could be further investigated for further *in vivo* tests.

3.5.2. Bioimaging

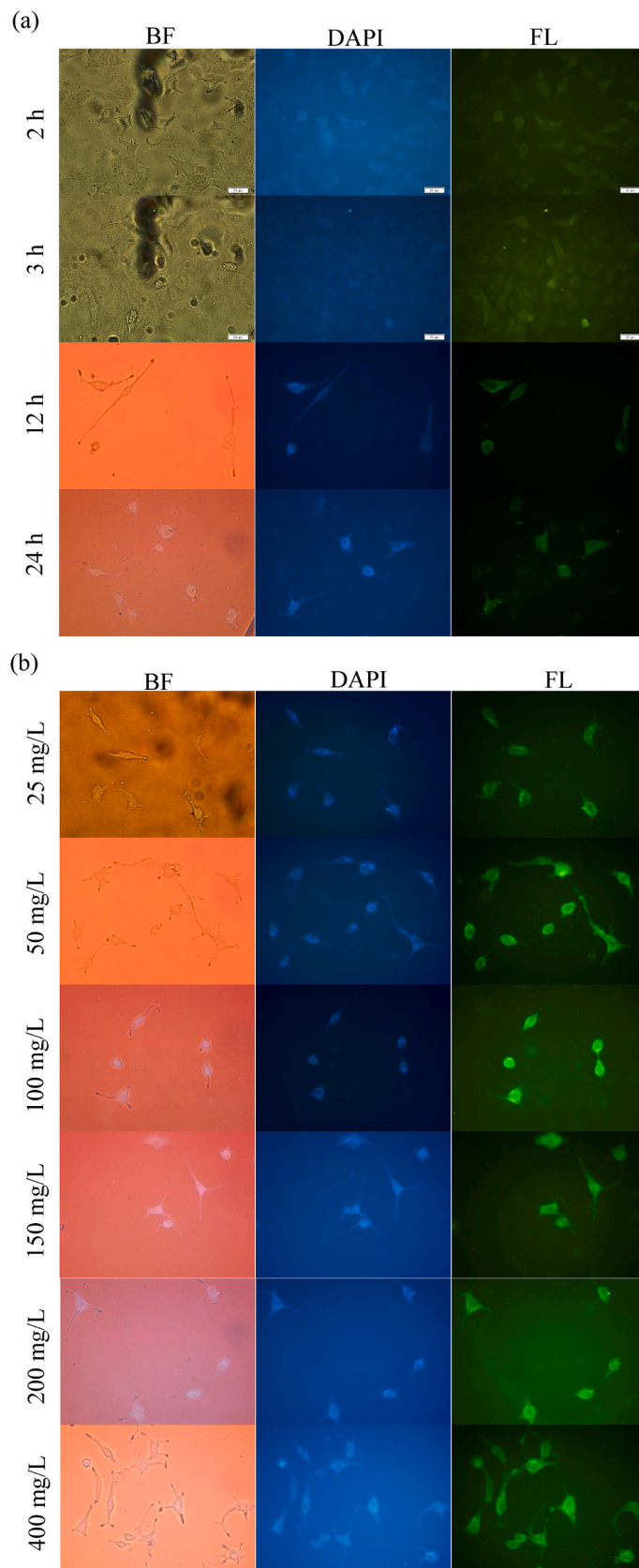
FA targeting ability of SiQDs/KCC-1-NH₂@SiO₂/FA was assessed by comparison of the amount of cellular uptake between MCF 7 (as FR-overexpressed cells) [39] and HEK 293 (as low-expressed cells) [40,41]. Fig. 4a demonstrates the fluorescent microscopic images of MCF 7 cancer cells after incubation with the SiQDs/KCC-1-NH₂@SiO₂/FA nanocomposite for 2, 3, 4, 12, and 24 h in the RPMI media. The morphology of the MCF 7 cell is nearly unaffected after even 24 h of treatment with the as-prepared materials. Also, the aggregate form of SiQDs/KCC-1-NH₂@SiO₂/FA is presented in bright green. When SiQDs/KCC-1-NH₂@SiO₂/FA are anchored into FR-overexpressed MCF 7 cells via the interaction of FA and FR, the location of the host cells can be detected by a fluorescence microscope.

The SiQDs/KCC-1-NH₂@SiO₂/FA emitted green emission luminescence after attaching to the surface of the cells. The uptake efficiency of SiQDs/KCC-1-NH₂@SiO₂/FA is enhanced upon progressing the time of incubation. Bright green emission was identified in the cytoplasm and surface membrane of the cells, but not in the nucleus, indicating that the SiQDs/KCC-1-NH₂@SiO₂/FA remain in the membrane and progressively diffuse into the cytoplasm of MCF-7 cells. This phenomenon is based on the hypothesis of the availability of FR on the membrane of the cells. The auto-fluorescence of control groups was not observed in non-stained cells (see Scheme 2).

Cellular internalization of the SiQDs/KCC-1-NH₂@SiO₂/FA was not favorable after 3 h of incubation; however, the internalization of the nanoparticles was enhanced by the time of incubation. Besides, the internalization percentages are proportional to the concentration of nanoparticles. In fact, the higher concentration of SiQDs/KCC-1-NH₂@SiO₂/FA means the enhanced number of interactions among FRs of the cell membrane and FA of the nanoparticles.

Fig. 4b shows the result of the incubation of MCF 7 cancer cells with 25, 50, 100, 150, 200 and 400 μ g/mL of SiQDs/KCC-1-NH₂@SiO₂/FA. Results implied that after adding 50 μ g/mL of the nanoparticles, the fluorescence intensity remained constant (Fig. 4b).

Fluorescence microscopy provides the quantitative results which could be used for visual comparison between control and case groups. To provide more precise findings, flow cytometry technique is usually employed. In this regard, the internalization ability of SiQDs/KCC-1-NH₂@SiO₂/FA with this technique is studied and the obtained results are shown in F. 9S. This figure can obviously



(caption on next page)

Fig. 4. Visual internalization of SiQDs/KCC-1-NH₂@SiO₂/FA to FR-positive cells at (a) various times of incubation in the presence of 200 µg/mL of NPs and (b) concentrations at the incubation time of 12 h (Scale bar: 40 µm, BF: bright field, DAPI: (4',6-diamidino-2-phenylindole), and FL: fluorescence).

confirm the high level of uptake of SiQDs/KCC-1-NH₂@SiO₂/FA with the MCF 7 cells. Total uptake values of the nanoparticles were 4% and 58% for 10 µg/mL and 200 µg/mL after about 6 h of incubation time.

3.5.3. Imaging specificity

The targeting capacity of the SiQDs/KCC-1-NH₂@SiO₂/FA nanocomposites was studied by fluorescence microscopy with the incubation of HEK 293 cells with the nanoparticles [42]. Bioimaging results implied that the SiQDs/KCC-1-NH₂@SiO₂/FA failed to anchor to the HEK 293 cells because of low expression of FRs, showing the targeted manner of the nanocomposite. The high affinity of SiQDs/KCC-1-NH₂@SiO₂/FA to FRs of MCF 7 cell membrane is mainly caused by high strength of FA/FRs bond with a dissociation constant of about 0.1–1 nM, resulting in the targeted attachment and bioimaging of the cells. F. 10S demonstrates the specific manner of SiQDs/KCC-1-NH₂@SiO₂/FA towards the breast cancer cells.

4. Conclusion

In the present study, FA-functionalized silica-based materials *i.e.* SiQDs/KCC-1-NH₂@SiO₂/FA, was employed for targeting MCF 7 breast cell via FA/FR interactions. The produced nanoparticles are biocompatible materials with high QY, large Stokes shift and bright fluorescence. The cell viability of SiQDs/KCC-1-NH₂@SiO₂/FA nanocomposite was proved by MTT assay with a biocompatible concentration of about 200 mg/L. Obtained results revealed that SiQDs/KCC-1-NH₂@SiO₂/FA nanoparticles could internalize to the breast cancer cells through surface receptors with excellent specificity. These results were confirmed by fluorescence microscopy and flow cytometry as qualitative and quantitative methods, respectively. As a limitation, the KCC-1 dispersions must be sufficiently agitated and sonicated to be a monodispersed material for bioimaging. In brief, the produced nanomaterial is a very potent material from biocompatibility, cell targeting ability, and bright fluorescence emission points of view. It is proposed for the fabrication of future *in vivo* bioimaging devices.

Author contribution statement

Yalda Zare Performed the experiments, Analyzed and interpreted the data.

Maral Maghsoudi-Salek Performed the experiments, Analyzed and interpreted the data.

Zahra Golsanmalou Performed the experiments, Analyzed and interpreted the data, Wrote the paper.

Abolghasem Jouyban Conceived and designed the experiments, Analyzed and interpreted the data.

Jafar Soleymani Conceived and designed the experiments, Analyzed and interpreted the data, Wrote the paper.

Hassan Bagherpour-Shamloo Performed the experiments, Analyzed and interpreted the data.

Funding statement

Dr Jafar Soleymani was supported by Tabriz University of Medical Sciences [67984].

Data availability statement

Data included in article/supp. material/referenced in article.

Declaration of interest's statement

The authors declare no competing interests.

Appendix A. Supplementary data

Supplementary data related to this article can be found at <https://doi.org/10.1016/j.heliyon.2023.e13207>.

References

- [1] W. Zhang, F. Wang, C. Hu, Y. Zhou, H. Gao, J. Hu, The progress and perspective of nanoparticle-enabled tumor metastasis treatment, *Acta Pharm. Sin. B.* 10 (2020) 2037–2053, <https://doi.org/10.1016/j.apsb.2020.07.013>.
- [2] R.L. Siegel, K.D. Miller, A. Jemal, *Cancer statistics, 2020*, CA, *Cancer J. Clin.* 70 (2020) 7–30, <https://doi.org/10.3322/caac.21590>.
- [3] L. Zhu, X. Feng, S. Yang, J. Wang, Y. Pan, J. Ding, C. Li, X. Yin, Y. Yu, Colorimetric detection of immunomagnetically captured rare number CTCs using mDNA-wrapped single-walled carbon nanotubes, *Biosens. Bioelectron.* 172 (2021), 112780, <https://doi.org/10.1016/j.bios.2020.112780>.

- [4] Y. Yang, Y. Fu, H. Su, L. Mao, M. Chen, Sensitive detection of MCF-7 human breast cancer cells by using a novel DNA-labeled sandwich electrochemical biosensor, *Biosens. Bioelectron.* 122 (2018) 175–182, <https://doi.org/10.1016/j.bios.2018.09.062>.
- [5] M. Hasanazadeh, S. Rahimi, E. Solhi, A. Mokhtarzadeh, N. Shadjou, J. Soleymani, S. Mahboob, Probing the antigen-antibody interaction towards ultrasensitive recognition of cancer biomarker in adenocarcinoma cell lysates using layer-by-layer assembled silver nano-cubics with porous structure on cysteamine capped QDs, *Microchem. J.* 143 (2018) 379–393, <https://doi.org/10.1016/j.microc.2018.08.028>.
- [6] B. Khalilzadeh, N. Shadjou, H.N. Charoudeh, M.-R. Rashidi, Recent advances in electrochemical and electrochemiluminescence based determination of the activity of caspase-3, *Microchim. Acta* 184 (2017) 3651–3662, <https://doi.org/10.1007/s00604-017-2466-y>.
- [7] B. Khalilzadeh, M. Rashidi, A. Soleimani, H. Tajalli, G.S. Kanberoglu, B. Baradaran, M.-R. Rashidi, Development of a reliable microRNA based electrochemical genosensor for monitoring of miR-146a, as key regulatory agent of neurodegenerative disease, *Int. J. Biol. Macromol.* 134 (2019) 695–703, <https://doi.org/10.1016/j.ijbiomac.2019.05.061>.
- [8] R. Awasthi, A. Roseblade, P.M. Hansbro, M.J. Rathbone, K. Dua, M. Bewawy, Nanoparticles in cancer treatment: opportunities and obstacles, *Curr. Drug Targets* 19 (2018) 1696–1709, <https://doi.org/10.2174/1389450119666180326122831>.
- [9] E.A. Owens, M. Henary, G. El Fakhri, H.S. Choi, Tissue-specific near-infrared fluorescence imaging, *Acc. Chem. Res.* 49 (2016) 1731–1740, <https://doi.org/10.1021/acs.accounts.6b00239>.
- [10] R. Pourakbari, N. Shadjou, H. Yousefi, I. Isildak, M. Yousefi, M.-R. Rashidi, B. Khalilzadeh, Recent progress in nanomaterial-based electrochemical biosensors for pathogenic bacteria, *Microchim. Acta* 186 (2019) 820, <https://doi.org/10.1007/s00604-019-3966-8>.
- [11] Y. Braeken, S. Cheruku, A. Ethirajan, W. Maes, Conjugated polymer nanoparticles for bioimaging, *Materials* 10 (2017) 1420, <https://doi.org/10.3390/ma10121420>.
- [12] C.R. Patra, S. Mukherjee, R. Kotcherlakota, Biosynthesized silver nanoparticles: a step forward for cancer theranostics? *Nanomedicine* 9 (2014) 1445–1448, <https://doi.org/10.2217/nmm.14.89>.
- [13] R. Liu, J. Zhao, G. Han, T. Zhao, R. Zhang, B. Liu, Z. Liu, C. Zhang, L. Yang, Z. Zhang, Click-functionalized sers nanoprobe with improved labeling efficiency and capability for cancer cell imaging, *ACS Appl. Mater. Interfaces* 9 (2017) 38222–38229, <https://doi.org/10.1021/acsami.7b10409>.
- [14] O. Sijilmassi, Folic acid deficiency and vision: a review, *Graefes Arch. Clin. Exp. Ophthalmol.* 257 (2019) 1573–1580, <https://doi.org/10.1007/s00417-019-04304-3>.
- [15] J. Qian, F. Quan, F. Zhao, C. Wu, Z. Wang, L. Zhou, Aconitic acid derived carbon dots: conjugated interaction for the detection of folic acid and fluorescence targeted imaging of folate receptor overexpressed cancer cells, *Sens. Actuators, B* 262 (2018) 444–451, <https://doi.org/10.1016/j.snb.2018.01.227>.
- [16] J. Soleymani, M. Hasanazadeh, N. Shadjou, M.H. Somi, A. Jouyban, The role of nanomaterials on the cancer cells sensing based on folate receptor: analytical approach, *TrAC, Trends Anal. Chem.* 125 (2020), 115834, <https://doi.org/10.1016/j.trac.2020.115834>.
- [17] B. Farran, E. Pavitra, P. Kasa, S. Peela, G.S. Rama Raju, G.P. Nagaraju, Folate-targeted immunotherapies: passive and active strategies for cancer, *Cytokine Growth Factor Rev.* 45 (2019) 45–52, <https://doi.org/10.1016/j.cytogfr.2019.02.001>.
- [18] M. Fernandez, F. Javaid, V. Chudasama, Advances in targeting the folate receptor in the treatment/imaging of cancers, *Chem. Sci.* 9 (2018) 790–810, <https://doi.org/10.1039/C7SC04004K>.
- [19] L. He, Q. Pagneux, I. Larroulet, A.Y. Serrano, A. Pesquera, A. Zurutuza, D. Mandler, R. Boukherroub, S. Szunerits, Label-free femtomolar cancer biomarker detection in human serum using graphene-coated surface plasmon resonance chips, *Biosens. Bioelectron.* 89 (2017) 606–611, <https://doi.org/10.1016/j.bios.2016.01.076>.
- [20] S. Aiyer, R. Prasad, M. Kumar, K. Nirvikar, B. Jain, O.S. Kushwaha, Fluorescent carbon nanodots for targeted in vitro cancer cell imaging, *Appl. Mater. Today* 4 (2016) 71–77, <https://doi.org/10.1016/j.apmt.2016.07.001>.
- [21] J. Soleymani, M. Hasanazadeh, N. Shadjou, M.H. Somi, A. Jouyban, Spectrofluorimetric cytosensing of colorectal cancer cells using terbium-doped dendritic fibrous nano-silica functionalized by folic acid: a novel optical cytosensor for cancer detection, *J. Pharm. Biomed. Anal.* 180 (2020), 113077, <https://doi.org/10.1016/j.jpba.2019.113077>.
- [22] J. Soleymani, M. Hasanazadeh, M.H. Somi, A. Jouyban, Differentiation and targeting of HT 29 cancer cells based on folate bioreceptor using cysteamine functionalized gold nano-leaf, *Mater. Sci. Eng., C* 107 (2020), 110320, <https://doi.org/10.1016/j.msec.2019.110320>.
- [23] S. Zhao, S. Sun, K. Jiang, Y. Wang, Y. Liu, S. Wu, Z. Li, Q. Shu, H. Lin, In situ synthesis of fluorescent mesoporous silica-carbon dot nanohybrids featuring folate receptor-overexpressing cancer cell targeting and drug delivery, *Nano-Micro Lett.* 11 (2019) 32, <https://doi.org/10.1007/s40820-019-0263-3>.
- [24] S. Damiati, M. Peacock, R. Mhanna, S. Sopstad, U.B. Sleytr, B. Schuster, Bioinspired detection sensor based on functional nanostructures of S-proteins to target the folate receptors in breast cancer cells, *Sens. Actuators, B Chem.* 267 (2018) 224–230, <https://doi.org/10.1016/j.snb.2018.04.037>.
- [25] W. Cheng, J. Nie, L. Xu, C. Liang, Y. Peng, G. Liu, T. Wang, L. Mei, L. Huang, X. Zeng, pH-sensitive delivery vehicle based on folic acid-conjugated polydopamine-modified mesoporous silica nanoparticles for targeted cancer therapy, *ACS Appl. Mater. Interfaces* 9 (2017) 18462–18473, <https://doi.org/10.1021/acsami.7b02457>.
- [26] J. Soleymani, M. Hasanazadeh, M.H. Somi, N. Shadjou, A. Jouyban, Probing the specific binding of folic acid to folate receptor using amino-functionalized mesoporous silica nanoparticles for differentiation of MCF 7 tumoral cells from MCF 10A, *Biosens. Bioelectron.* 115 (2018) 61–69, <https://doi.org/10.1016/j.bios.2018.05.025>.
- [27] S.M. Sadeghzadeh, R. Zhiyani, M. Khoobi, S. Emrani, Synthesis of 3-Acyloxyindolines under mild conditions using triphosphosphate-grafted KCC-1-NH₂, *Microporous Mesoporous Mater.* 257 (2018) 147–153, <https://doi.org/10.1016/j.micromeso.2017.08.037>.
- [28] Z. Golsanamlou, J. Soleymani, S. Abbaspour, M. Siah-Shadbad, E. Rahimpour, A. Jouyban, Sensing and bioimaging of lead ions in intracellular cancer cells and biomedical media using amine-functionalized silicon quantum dots fluorescent probe, *Spectrochim. Acta Part A Mol. Biomol. Spectrosc.* 256 (2021), 119747, <https://doi.org/10.1016/j.saa.2021.119747>.
- [29] N. Bayal, B. Singh, R. Singh, V. Polshettiwar, Size and fiber density controlled synthesis of fibrous nanosilica spheres (KCC-1), *Sci. Rep.* 6 (2016), 24888, <https://doi.org/10.1038/srep24888>.
- [30] V. Polshettiwar, D. Cha, X. Zhang, J.M. Basset, High-surface-area silica nanospheres (KCC-1) with a fibrous morphology, *Angew. Chem., Int. Ed.* 49 (2010) 9652–9656, <https://doi.org/10.1002/anie.201003451>.
- [31] K.E.A. AbouAitah, A.A. Farghali, A. Swiderska-Sroda, W. Lojkowski, A.M. Razin, M.K. Khedr, Mesoporous silica materials in drug delivery system: pH/glutathione-responsive release of poorly water-soluble pro-drug quercetin from two and three-dimensional pore-structure nanoparticles, *J. Nanomed. Nanotechnol.* 7 (2016) 351, <https://doi.org/10.4172/2157-7439.1000360>.
- [32] K. AbouAitah, A. Swiderska-Sroda, A.A. Farghali, J. Wojnarowicz, A. Stefanek, S. Gierlotka, A. Opalinska, A.K. Allayeh, T. Ciach, W. Lojkowski, Folic acid-conjugated mesoporous silica particles as nanocarriers of natural prodrugs for cancer targeting and antioxidant action, *Oncotarget* 9 (2018), 26466, <https://doi.org/10.18632/oncotarget.25470>.
- [33] S. Azizi, J. Soleymani, M. Hasanazadeh, Iron oxide magnetic nanoparticles supported on amino propyl-functionalized KCC-1 as robust recyclable catalyst for one pot and green synthesis of tetrahydropyrazolopyridines and cytotoxicity evaluation, *Appl. Organomet. Chem.* 10 (2020) 671–681, <https://doi.org/10.1002/aoc.5440>.
- [34] J. Wu, J. Dai, Y. Shao, Y. Sun, One-step synthesis of fluorescent silicon quantum dots (Si-QDs) and their application for cell imaging, *RSC Adv.* 5 (2015) 83581–83587, <https://doi.org/10.1039/c5ra13119g>.
- [35] P. Suppan, *Chemistry and Light*, The Royal Society of Chemistry, London, UK, 1994, <https://doi.org/10.1039/9781847550439>.
- [36] M. Jozefowicz, J.R. Heldt, Excitation-wavelength dependent fluorescence of ethyl 5-(4-aminophenyl)-3-amino-2,4-dicyanobenzoate, *J. Fluoresc.* 21 (2011) 239–245, <https://doi.org/10.1007/s10895-010-0711-4>.
- [37] X. Tang, H. Yu, B. Bui, L. Wang, C. Xing, S. Wang, M. Chen, Z. Hu, W. Chen, Nitrogen-doped fluorescence carbon dots as multi-mechanism detection for iodide and curcumin in biological and food samples, *Bioact. Mater.* 6 (2021) 1541–1554, <https://doi.org/10.1016/j.bioactmat.2020.11.006>.
- [38] J. Wu, J. Dai, Y. Shao, Y. Sun, One-step synthesis of fluorescent silicon quantum dots (Si-QDs) and their application for cell imaging, *RSC Adv.* 5 (2015) 83581–83587, <https://doi.org/10.1039/C5RA13119G>.

- [39] Z. Shen, Y. Li, K. Kohama, B. Oneill, J. Bi, Improved drug targeting of cancer cells by utilizing actively targetable folic acid-conjugated albumin nanospheres, *Pharmacol. Res.* 63 (2011) 51–58, <https://doi.org/10.1016/j.phrs.2010.10.012>.
- [40] S. Gorle, M. Ariatti, M. Singh, Novel serum-tolerant lipoplexes target the folate receptor efficiently, *Eur. J. Pharmaceut. Sci.* 59 (2014) 83–93, <https://doi.org/10.1016/j.ejps.2014.04.012>.
- [41] Y. Ji, X. Yang, Z. Ji, L. Zhu, N. Ma, D. Chen, X. Jia, J. Tang, Y. Cao, DFT-calculated IR spectrum amide I, II, and III band contributions of N-methylacetamide fine components, *ACS Omega* 5 (2020) 8572–8578, <https://doi.org/10.1021/acsomega.9b04421>.
- [42] K. Pal, A. Heinsch, A. Berkessel, A.L. Koner, Differentiation of folate-receptor-positive and -negative cells using a substrate-mimicking fluorescent probe, *Chem. Eur. J.* 23 (2017) 15008–15011, <https://doi.org/10.1002/chem.201703305>.